Amos Rantalainen

Enhancing Intelligence in Test Systems' Power Distribution Units

Metropolia University of Applied Sciences

Bachelor of Engineering

Electrical and Automation Engineering

Bachelor's Thesis

17 December 2024

Abstract

Author:	Amos Rantalainen
Title:	Enhancing Intelligence in Test Systems' Power Distribution Units
Number of Pages:	42 pages + 1 appendix
Date:	17 December 2024
Degree:	Bachelor of Engineering
Degree Programme:	Electrical and Automation Engineering
Professional Major:	Electronics
Supervisors:	Janne Mäntykoski, Senior Lecturer Teppo Myllys, Service Product Owner

---

The aim of this thesis work is to increase the Power Distribution Units' capabilities by adding intelligence to track power usage and provide valuable insights into the testing equipment's energy consumption patterns. The data collected will support PDU development by guiding a strategy to reduce the carbon footprint of test systems, lower operational costs, and promote sustainable practices in power distribution.

The prototype incorporated current sensors, a power meter, and a central hub to capture key metrics such as energy consumption, power factor and apparent power. Most of the software was developed in LabVIEW, while the C language was used for waveform capture, as it required fast data transfer speeds.

Through testing, it was observed that even when the test station remained idle, its passive consumption was relatively high, with small consumption peaks occurring during active use. The results also highlighted the potential need for adding power factor correction based on the captured waveforms and measured results. Possible improvements to the power distribution unit also include spreading the consumption equally across all three phases rather than leaving one largely unutilised.

Keywords: PDU, Data Capture, Power Consumption

Tiivistelmä

Tekijä:	Amos Rantalainen
Otsikko:	Älykkyyden kehittäminen testijärjestelmien virranjakeluyksikössä
Sivumäärä:	42 sivua + 1 liite
Aika:	17.12.2024
Tutkinto:	Insinööri (AMK)
Tutkinto-ohjelma:	Sähkö- ja automaatiotekniikka
Ammatillinen pääaine:	Elektroniikka
Ohjaajat:	Janne Mäntykoski, lehtori Teppo Myllys, palvelutuoteomistaja

Tämän insinöörityön tavoitteena on parantaa virransyöttöyksiköiden (PDU) toimintoja kehittämällä prototyyppi laitteesta, jonka avulla testausjärjestelmän energiankulutuskäyttäytymistä voidaan seurata. Seurannasta kerätyn datan avulla voidaan tehdä harkittuja päätöksiä virranjakeluyksikön kestävästä kehityksestä, tavoitteena vähentää hiilijalanjälkeä ja kuluja.

Prototyyppi koostui virta-antureista, tehomittarista ja keskusyksiköstä, jonka avulla energiankulutusta, tehokerrointa ja näennäistehoa saatiin mitattua. Mittaukset toteutettiin pääasiassa LabVIEW:llä kirjoitetun ohjelman avulla, mutta aaltomuotojen keräämiseen tarvittavan nopean tiedonsiirron vuoksi kommunikointi analogia-digitaalimuuntimen kanssa toteutettiin C-kielellä.

Testauksen aikana havaittiin testausaseman suuri passiivinen kulutus, johon verrattuna aktiivisessa käytössä syntyneet kulutushuiput olivat suhteessa pieniä. Saatu data mitatuista aaltomuodoista ja tehomittarin tuloksista toi esille myös tarpeen parantaa tehokerrointa. Virranjakeluyksikön kehityksessä tulee jatkossa myös kiinnittää huomiota tehon jakautumiseen tasaisesti kaikille kolmelle vaiheelle sen sijaan, että yksi vaihe jäisi suurimman osan ajasta kokonaan käyttämättä.

Avainsanat: PDU, datankeruu, tehonkulutus

Contents

List of Abbreviations

AC: Alternating Current

ADC: Analog to Digital Converter

C: General-purpose programming language.

CB: Control Block

CHP: Combined Heat and Power. A system that simultaneously generates electricity and usable heat.

$CO_{2:}$ Carbon Dioxide

CS: Chip Select. A control signal used to enable specific devices on a shared bus.

CT: Current Transformer. Used for measuring alternating current by stepping it down proportionally.

DC: Direct Current

DHCP: Dynamic Host Configuration Protocol. Automatically assigns IP addresses to devices on a network.

DMA: Direct Memory Access. Allows hardware to access system memory directly for faster data transfer.

EMF: Electromotive Force. The voltage generated by a source such as a battery or generator.

GPIO: General Purpose Inputs and Outputs. Programmable pins on a microcontroller or computer.

LabVIEW: Laboratory Virtual Instrument Engineering Workbench. Visual programming language based on g.

LEED: Leadership in Energy and Environmental Design. A certification program for sustainable building design.

MicroSD: A compact memory card used for data storage in portable devices.

MISO: Main In, Sub Out. A data line for sending information from a sub to the main in SPI communication.

Modbus RS485: Half-duplex data protocol commonly used in industrial automation for serial communication.

MOSI: Main Out, Sub In. A data line for sending information from the main to the sub in SPI communication.

MSB: Most Significant Bit. The highest-order bit in a binary number.

PCB: Printed Circuit Board

PDU: Power Distribution Unit. A device that distributes electrical power to multiple devices in a rack or system.

Raspberry Pi: A tiny single-board computer developed by the Raspberry Pi Foundation.

SCLK: Serial Clock. Used to synchronise data transfer in SPI communication.

SPI: Serial Peripheral Interface. A protocol for high-speed communication between devices.

SSH: Secure Shell. A protocol for securely accessing and managing remote systems over a network.

UPS: Uninterruptible Power Supply

USB: Universal Serial Bus

VA: Volt-Amps. A measure of apparent power in an electrical system.

VAR: Volt-Amps Reactive. A measure of reactive power in AC systems.

VI: Virtual Instrument, the basic building block of LabVIEW programs written in the G Language.

1 Introduction

Power Distribution Units (PDUs) are crucial in managing and distributing electrical power in various settings, from data centres to industrial environments. As the demand for energy-efficient systems grows, understanding and optimising power consumption has become essential for operational efficiency and environmental sustainability.

This thesis work focuses on designing, implementing, and evaluating methods for accurately measuring a test station’s power consumption. The goal is establishing a framework for more effective power monitoring and management. This is crucial for reducing energy costs, calculating standby power usage and climate impact, and ensuring optimal system performance.

The study analyses measurement techniques, their accuracy, and their impact on the preexisting design. It also explores the importance of real-time monitoring in enhancing power systems' reliability and considers emerging technologies' role in improving energy efficiency.

This study analyses power usage patterns in PDUs, providing valuable insights for large-scale operations and smaller industrial setups. Findings address the increasing demand for efficient energy management and the rising costs associated with continuously powered devices.

2 Costs Associated with Test Systems

The total cost of automated test systems encompasses multiple stages: development, deployment, and operational phases, each contributing to the overall expense. Development costs are typically the smallest and include planning, training, tool acquisition, and the initial development of hardware and software. Deployment costs rise significantly when scaling up for full production. Key factors include the number of test systems required, assembly and configuration time, and the logistics of moving systems to the production site. [1, 4-5.]

Power consumption significantly contributes to the long-term operating costs of automated test systems in manufacturing. As seen in Figure 1, this factor falls under operational expenses, which include the direct energy used to run the equipment and any cooling or ventilation systems needed to maintain proper system temperatures. High power demands may even require specialised electrical infrastructure, such as dedicated power lines or cooling towers, further increasing initial installation and ongoing maintenance costs. [1, 6.]

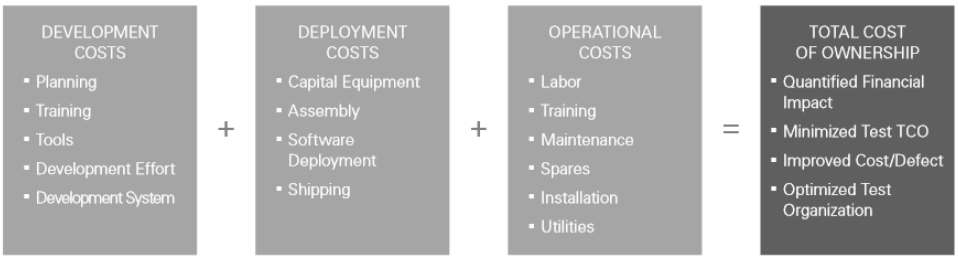

Figure 1. Total Cost of Ownership of a Test System [1, 3].

Utilities also encompass the footprint of test equipment on the manufacturing floor, where higher power consumption might correlate with larger, more energy-intensive setups, leading to additional costs. Understanding and optimising power consumption in automated test systems is essential to minimising direct energy expenses and the broader implications for infrastructure, cooling requirements, and space utilisation, each contributing substantially to the overall operational expenditure. [1, 3.]

This aspect is frequently managed by the manufacturing or production team rather than the original R&D team, reflecting a common separation in cost centres. When manufacturing is outsourced, the contract manufacturer typically handles these utility costs, often negotiating a flat rate. This further emphasises power consumption's impact on the total cost of ownership [1, 3].

2.1 Power Distribution Unit

A PDU is crucial for managing electrical power distribution across multiple devices from a single source. By running power through a centralised unit, PDUs can reduce energy costs by centralising and controlling the flow of electricity. This efficiency is critical in industrial environments, where numerous devices run simultaneously, allowing for better energy management and lower operational costs. [2.]

PDUs also enhance reliability by providing a stable source of power, which helps prevent fluctuations or outages caused by inconsistent or overloaded individual power sources. Acting as a stable power source for critical equipment, PDUs and Uninterruptible Power Supplies (UPS) work together to ensure uninterrupted operations and reduce the risk of disruptions. [2.]

In addition to energy efficiency and reliability, PDUs contribute to better organisation and easier installation. Acting as a central hub, they minimise cable clutter and optimise rack space utilisation, simplifying power management. They are compatible with various plug standards, making them versatile and adaptable to different power requirements across various settings. PDUs can be found in multiple variations (Figure 2). [2.]

Figure 2. Generic PDUs [3].

The development PDU is integrated into a 19” rack housing to supply power to all other devices mounted on the test station. It features a basic control panel with power switches, fuses, and Light-Emitting Diode (LED) indicators for status monitoring (Figure 3).

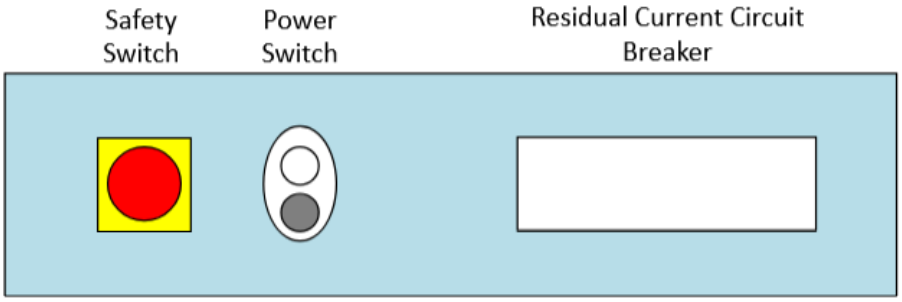

Figure 3. PDU Front Side.

At the back of the PDU is a single power input and multiple outputs (Figure 4).

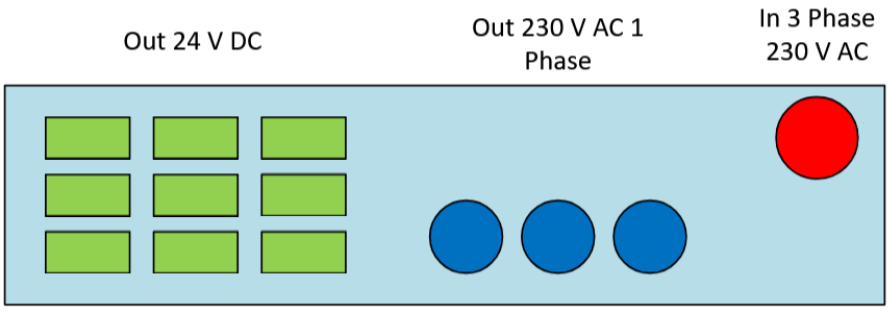

Figure 4. PDU Back Side.

Depending on the tester configuration, most outputs are connected directly to other testing instruments. However, for the most critical equipment, the power is routed through an Uninterruptible Power Supply (UPS), which provides protection against power fluctuations and ensures continuous operation for the most valuable devices. Figure 5 below is a typical testing station housing a PDU. The PDU is mounted at the top of the rack, while the UPS is at the bottom.

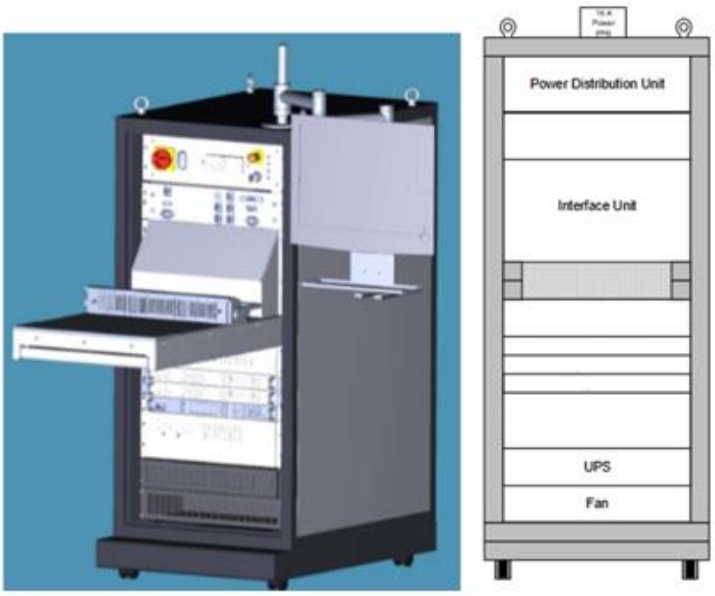

Figure 5. 3D (Left) and 2D (Right) Models of a Typical Test Station That Utilizes a PDU.

2.2 Existing PDU Evaluation

The current PDU model serves only as a basic power distributor. It handles a 3-phase 230 V AC (Alternating Current) input and supplies three 230 V AC outputs and multiple 24 V DC (Direct Current) outputs.

Energy monitoring is the primary area for improvement, as it could play a critical role in reducing costs and emissions. Although the PDU lacks built-in intelligence and cannot currently track power consumption, it provides internal power sources that could support the integration of measurement equipment.

Proper data on these testers' power consumption or carbon footprint is yet to be collected. However, internal estimates suggest that the testing equipment

generates CO_2 emissions comparable to or exceeding those produced during the testers' manufacturing. Given the limited solutions available, a plan has been proposed to redesign the PDU, incorporating features to address these issues effectively.

2.3 Uninterruptable Power Supply

A UPS backup system ensures critical devices keep running during power outages. Its main components include a rectifier/charger, batteries, inverter, static bypass, and control unit. It converts AC from the grid to DC for charging batteries and back to AC for connected devices. It switches to battery power during outages, ensuring uninterrupted service while filtering and stabilising electrical surges. UPS systems are crucial in power-critical environments, like hospitals and industrial facilities, providing stable power for essential operations. [4.]

3 KONE Oyj

KONE is a global elevator and escalator industry leader and plays a vital role in modern urban infrastructure by providing solutions for mass movement. Founded in 1910 and headquartered in Espoo, Finland, KONE designs, manufactures, installs, and maintains elevators, escalators, and automatic building doors. [5.]

Operating in over 60 countries with a workforce of more than 60,000 employees, KONE is known for its safe, efficient, and eco-friendly systems. As urbanisation accelerates, KONE’s products are critical for addressing the growing need for vertical mobility, particularly in high-rise buildings and densely populated urban areas. [5.]

3.1 Sustainability at KONE

KONE emphasises eco-efficiency in its products, such as the KONE MonoSpace® elevator, designed to reduce energy consumption and environmental impact. The company collaborates with builders to achieve

sustainability certifications like Leadership in Energy and Environmental Design (LEED), promoting greener urban environments. Additionally, KONE's modernisation services enhance the lifespan and safety of ageing infrastructure, contributing to sustainable urban development amid growing urbanisation. [6.]

3.2 Testing at KONE

Testing at KONE ensures systems' safety, reliability, and performance worldwide. It covers both individual components and entire systems, including hardware and software. KONE’s testing facilities are located globally, with key operations in Finland, India, and the US. As technology evolves, AI, IoT, and digital twins are increasingly used to improve remote and virtual testing. However, real-world hardware testing, such as at the Tytyri facility, remains essential for validating conditions that simulations cannot fully replicate. [7.]

4 Measuring Power Consumption

Electricity is measured in units called Watts. A watt is the electrical power equivalent to one ampere under one volt. While small devices typically consume a few Watts (W), the power consumption of larger devices is measured in kilowatts. [8.]

Energy consumption is quantified in Watthours, which indicates energy equivalent to watts supplied over one hour. The kilowatt-hour is the standard unit for measuring household and business electricity usage, representing one kilowatt consumed over one hour. Accurate electricity consumption measurement is vital for efficient energy management in homes and businesses. Understanding power usage helps reduce costs and supports sustainability efforts. [8.]

4.1 Real Power

In AC circuits, real power represents the actual power consumed or dissipated and is measured in Watts, denoted by the symbol P. This power reflects the

energy resistive components use to perform work, such as lighting a bulb or heating an element. However, AC circuits are more complex due to the phase difference θ between current and voltage. The average value of real power is given by the equation (1). [9.]

$$P = VI\cos\theta \quad (1)$$

Where $\cos\theta$ accounts for the phase difference. [9.]

4.2 Reactive Power

Reactive power (Q) refers to the power that continuously bounces back and forth between the source and load. This type of power is merely absorbed and returned in the load due to its reactive properties. It arises in circuits with inductive and capacitive loads, which do not dissipate real power despite drawing current and affecting voltage. Often referred to as "phantom power," reactive power is measured in Volt-Amps-Reactive (VAR) and is symbolised by the letter Q. [10.]

While reactive power does not contribute to the actual work done in the circuit, it is essential for maintaining voltage levels within the system. Reactive power represents energy that is first stored and then released as magnetic fields in inductors and electrostatic fields in capacitors. It can be calculated using the equation (2), yielding positive values for inductive loads and negative values for capacitive loads.

$$Q = \mathrm{VI}\sin\theta \quad (2)$$

Where $\sin\theta$ accounts for the phase difference. [11.]

4.3 Apparent Power

Apparent power, denoted by S and measured in Volt-Amps, is the product of the root mean square (RMS) voltage and the RMS current in an AC circuit, ignoring

any phase angle differences between current and voltage. It represents the total power in an AC circuit, encompassing both the power that is dissipated and the power that is absorbed or returned. Apparent power is the combination of reactive and true power, and its unit of measurement is defined as VA. In circuits with purely resistive loads, the apparent power is equal to the real or true power. However, in circuits with inductive or capacitive loads, where reactance is present, the apparent power exceeds the real or true power. [9.]

4.4 Mathematical Representations

The real, reactive, and apparent power calculations use scalar quantities to represent voltage, current, and impedance. For accurate calculations, voltage and current must be expressed in their polar magnitudes. The relationships between real, reactive, and apparent power can be visualised using a power triangle (Figure 6), where real (true) power (P) forms the adjacent side, reactive power (Q) forms the opposite side, and apparent power (S) is the hypotenuse. The angle opposite the reactive power side corresponds to the phase angle of the circuit's impedance (Z). [10.]

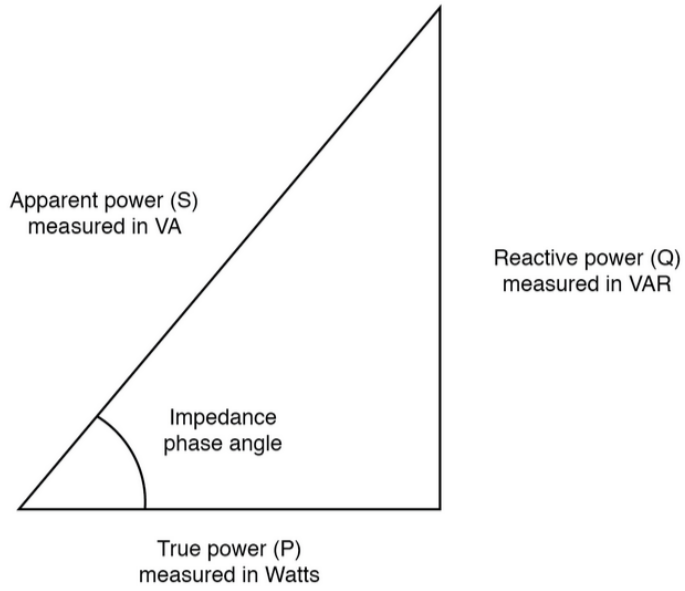

Figure 6. Power Triangle [10].

4.5 Single and Three-phase Power

In electrical systems, phase refers to how electrical loads are distributed. Single-phase and three-phase power supplies are the two most common configurations for delivering electricity. A single-phase power supply consists of two wires: one phase wire and one neutral wire. This type of power is typical for residential applications where the primary loads are lighting, heating, and smaller appliances. The voltage in a single-phase system rises and falls in a sinusoidal pattern, creating peaks and dips in power delivery and affecting consistency. [12.]

On the other hand, a three-phase power supply uses three wires, each carrying its own AC signal, with each phase 120 degrees apart. This system is generally used in commercial and industrial settings since it can handle larger electrical loads, such as heavy machinery and large motors. One key advantage of three-phase systems is that they provide a more constant and balanced power flow (Figure 7). As the three phases alternate, power delivery is even, minimising dips in voltage and making it more suitable for demanding equipment. [12.]

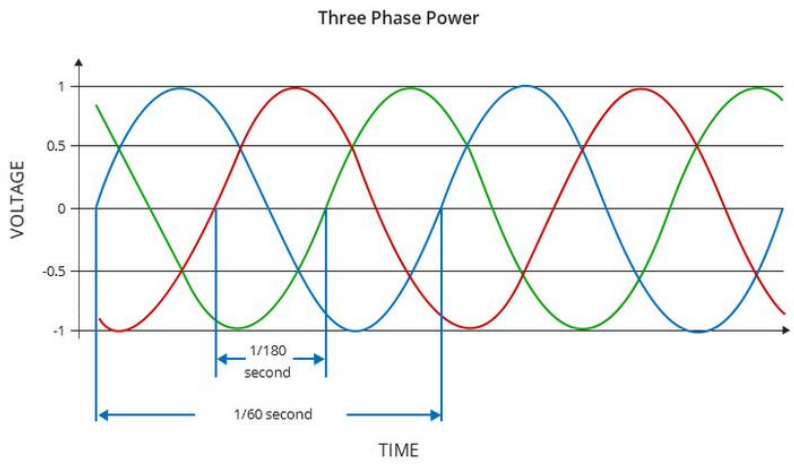

Figure 7. 3 Phase AC Power [13].

Another notable difference between single-phase and three-phase systems is efficiency. A three-phase system can deliver up to three times the power of a single-phase system while requiring only one additional conductor. This wire is

often paired with a neutral wire, bringing the total to four, as shown in the wye configuration below (Figure 8). [13.]

Three-phase systems do not require a neutral wire to return power to the grid when wired like in the delta configuration (Figure 8). Instead, the system's balanced nature allows each phase to serve as a return path for the others, enabling current to flow back efficiently without a dedicated return wire. [15.]

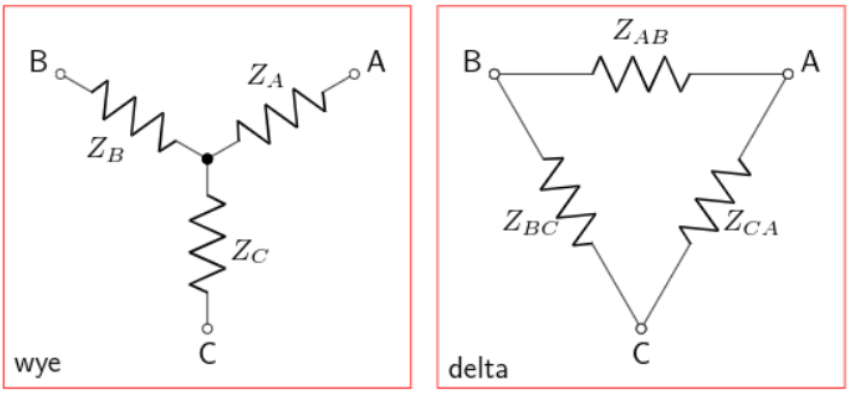

Figure 8. Four- (left) and Three-wire (right) System [15].

4.6 Power Factor Corrector

Power factor correction (PFC) is the ratio of real power to apparent power (3). If both current and voltage are sinusoidal and perfectly in phase, the power factor is 1.0. When the waveforms are sinusoidal but out of phase, the power factor becomes the cosine of the phase angle between them. This phase-angle-based definition only holds when current and voltage are pure sine waves. [16, 9.]

$$PF = \frac{Real\ Power\ (W)}{Apparent\ Power\ (VA)} \quad (3)$$

4.7 Calculating Carbon Footprint from Electrical Power Consumption

The real-time CO_2 emission calculation for Finland's electricity system is based on real-time production, import, and export data from Fingrid's monitoring system, alongside predefined emission factors. The calculation considers Hydro, nuclear,

wind, and solar power emission-free. For combined heat and power (CHP) plants, emission factors are derived from Tilastokeskus‘s electricity and heat production data. Emissions from the separate production within CHP plants are included in the CHP emission factors based on the energy share of each production type. [17.]

Emission factors for electricity imports are defined on a country-by-country basis and are constant values that are updated annually. These factors are based on historical production data reported by the International Energy Agency (IEA), which has set country-specific emission factors for Sweden, Norway, Russia, and Estonia. In the case of imports, only the emission factor of the exporting country's electricity production is considered, with the import increasing the emissions related to Finland's electricity consumption. Finland's electricity production and imported electricity are considered for exports, with exports reducing the emissions linked to electricity consumed in Finland. For electricity consumed in Finland, emissions are calculated by considering domestic production, imports, and exports as shown in (4). [17.]

$$Domestic\ Consumption\ Emissions = \frac{Domestic\ Prod.\ +\ Import\ Prod.\ -Domestic\ Exp.}{Domestic + Imported\ -Exported} \quad (4)$$

5 Current Sensing Principles and Safe Operation

A thorough understanding of the underlying physics of current sensing was needed to select the correct components and accurately interpret the results.

5.1 Faraday’s Laws of Induction

Faraday’s Law of Induction is crucial in current-sensing devices such as current transformers (CTs). These sensors provide inherent electrical isolation, making them ideal for safe and accurate current measurements. [18.]

Faraday’s laws of electromagnetic induction explain how electromotive force (EMF) is generated when a conductor interacts with a magnetic field. His first law

states that an emf is induced in a conductor when it cuts through a magnetic field or when the magnetic flux linked to a circuit changes. However, no EMF is induced if the conductor moves parallel to the magnetic field without cutting through it. [19, 235-236.]

Faraday's second law further states that the magnitude of the induced emf is directly proportional to the rate of change of magnetic flux through a coil. This is mathematically expressed as the product of the change in flux and the number of turns in the coil divided by the time interval. Lenz's law complements this by stating that the induced EMF opposes the change in flux that caused it, ensuring energy conservation within the electromagnetic system. This opposition is reflected in the negative sign in the equation below (5). [19, 236.]

$$e = -N\frac{d\varphi}{dt}V \tag{5}$$

5.1.1 Toroidal Current Sense Transformer

A current sense transformer, or current transformer, is a specialised type used for measuring AC in a conductor while providing electrical isolation between the primary circuit and the measurement equipment. The primary winding is integrated into the main circuit, and a secondary winding produces a proportional current, which can be measured to determine the primary current. The current transformer operates on the principle of electromagnetic induction, with the ratio of primary to secondary turns dictating the current transformation. This allows precise current monitoring without requiring a direct electrical connection to the high-voltage circuit. [20.]

Current sense transformers come in various forms, such as toroidal (Figure 9), traditional wound, and bar transformers, each suited for different applications. Toroidal transformers are often used in clamp meters to allow non-invasive current measurement by clipping around an existing conductor. These transformers are essential in applications like power supply monitoring and ground fault detection, where electrical isolation and accurate, current sensing

are critical. Properly selecting a current transformer requires considering factors such as current levels, frequency range, and compatibility with the measuring equipment. [20.]

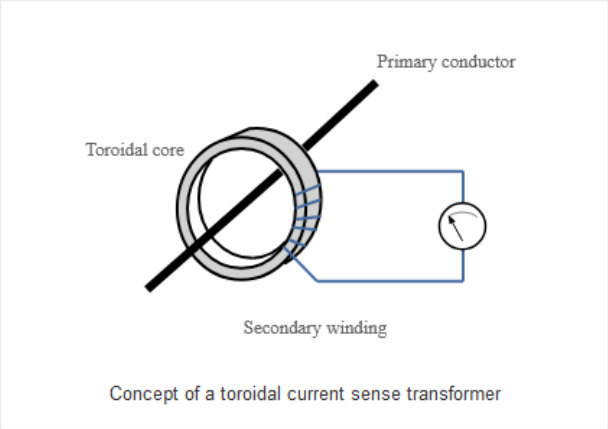

Figure 9. Toroidal Current Sense Transformer [20].

5.1.2 Hall-Effect Sensor

Hall-effect sensors work by detecting the density of the magnetic field around the device. The sensors have a present threshold, and when magnetic flux density exceeds the limit, the device will detect the magnetic field by generating an output called ‘Hall Voltage’. [21.]

Hall-effect sensors operate using a thin piece of semiconductor material through which a continuous electrical current flows, generating a magnetic field. When placed near an external magnet, the magnetic flux exerts a force on the semiconductor. This force causes electrons to move, generating a measurable Hall voltage, which activates the sensor. A simplified depiction of this can be seen below (Figure 10). [21.]

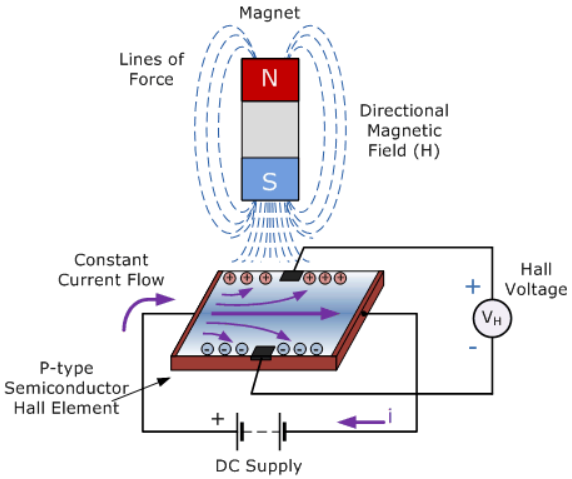

Figure 10. Hall-effect Sensor Principles [22].

The Hall voltage produced is directly proportional to the strength of the magnetic field interacting with the semiconductor. However, this output voltage is typically minimal, often only a few microvolts. To enhance the sensor's sensitivity and overall effectiveness, many Hall-effect devices include built-in DC amplifiers, logic-switching circuits, and voltage regulators (Figure 11). These components work together to improve the accuracy and performance of the sensor in detecting magnetic fields. [22.]

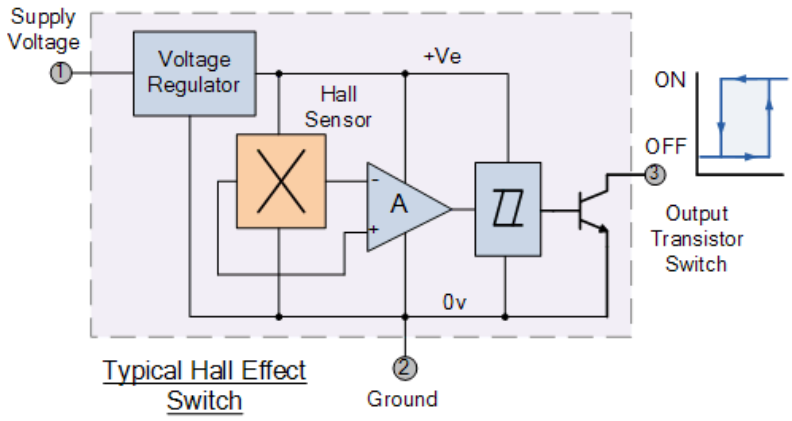

Figure 11. High-level Schematic of a Typical Hall-Effect Sensor [22].

5.2 Verifying Safe Operation

Incorrect or faulty wiring in the PDU poses a significant safety risk, potentially leading to injury or death. Therefore, it was critical during the design process to avoid interfering with existing safety mechanisms or introducing new hazards.

Additionally, a qualified individual with proper electrical safety training had to verify that the modified PDU met all safety standards and was correctly configured. Only after this verification could the device be safely powered on.

6 Intelligent PDU Development

The aim was to develop a functional device prototype to add intelligence to the PDU. The scale of this thesis work was limited to reading consumption while adding necessary IO for future development.

6.1 Development Approach

Before starting, key development practices were identified: safety, scalability, operational stability, and extensive data logging capabilities.

The design prioritised proper isolation, high-quality components, and a minimal number of high-voltage connections to ensure safety. Verifying the dead state of the PDU was crucial, and the emphasis was on taking the necessary time to avoid mistakes and prevent rushing through critical steps.

6.2 Hardware Development

The overall focus in hardware development was on mobility/disassembly, reduced interference with the preexisting design, and planning for the ability to continue development beyond the thesis work.

Modules that could connect to a DIN rail were preferred, as attaching one to the inside of the PDU was the ideal choice.

6.2.1 Microcontroller

Key considerations when selecting an appropriate microcontroller included availability and connectivity. While commonly used in similar contexts, the Raspberry Pi is not a microcontroller but a single-board computer [23]. Nevertheless, it can operate as a fully standalone device with full-sized Ethernet and USB ports.

The developed device required internal power from the PDU. Since the PDU only supplies 24 VDC, a buck converter was necessary to step down the voltage to 5 VDC to power the Raspberry Pi and the modules it supplied. A cost-effective DIN rail module with an adjustable output voltage was used and configured to deliver the required 5 VDC.

6.2.2 Selecting the Appropriate Current Sensor

Several factors were considered when selecting the current sensor to ensure optimal performance and compatibility. First, it was determined whether AC, DC, or both types of current needed to be measured. Some sensors, like current transformers, are explicitly designed for AC, while Hall-effect sensors can measure both [18].

Both Hall-effect and current transformer sensors were used in the PDU development. Current transformers were chosen for their ease of installation, as they could be clipped onto outgoing and incoming AC wires, whereas Hall-effect sensors required wiring through the sensor. Despite this, Hall-effect sensors remained less intrusive measurement options than, for example, shunt resistors and thus were used.

6.2.3 Converting and Scaling the Measured Signal

The Raspberry Pi lacks analogue input pins, so an Analog-to-Digital Converter (ADC) was required to convert the measured voltage from the current transformers and Hall-effect sensors. The chosen ADC needed sufficient input channels and a high sampling rate for complete measurements. To meet these requirements, a serial peripheral interface (SPI) -based ADC module powered by the AD7490 ADC was selected.

Since the ADC could only read voltages between 0 and 5 V, the incoming bipolar voltage had to be offset accordingly. By referencing the ADC's datasheet [24, 17], the incoming bipolar signals could be offset to the 0-5 V range. The circuit for offsetting the three input channels from the three current transformers and creating a stable reference voltage is shown below (Figure 12).

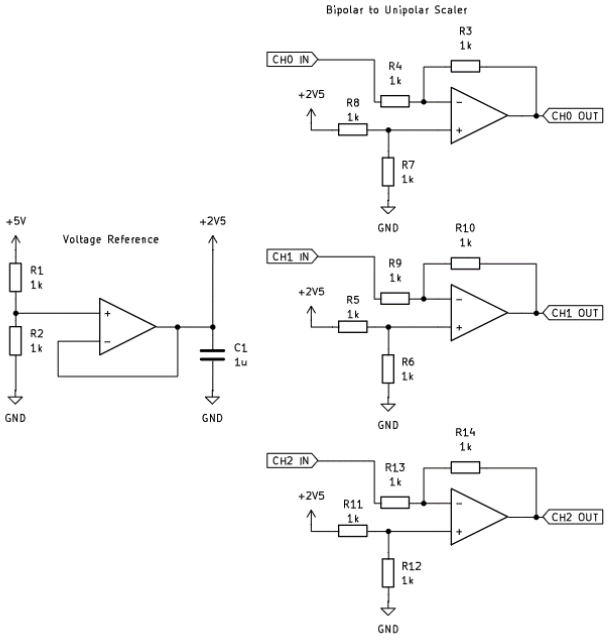

Figure 12. Offset Circuit for the Incoming Bipolar Voltage.

6.2.4 Measuring Mains Voltage

An off-the-shelf power meter module was the most suitable option for measuring stable, protected three-phase, four-wire mains voltage. This choice minimised clutter from unnecessary cables and fit within the PDU's tight space constraints.

Communication with this device was done using Modbus. As the Raspberry Pi lacks RS485 hardware support, this required using an external Modbus RS485 transceiver module attached to it. The module was connected to the Raspberry Pi's UART ports, enabling device communication.

When referring to Modbus RS485, it indicates using the Modbus protocol over RS485 serial transmission. Modbus defines the communication structure, while RS485 specifies the electrical signal levels. [25.]

6.2.5 Block Diagram

The device uses current sensors and a power measurement module to monitor consumption. The mains voltage is measured through the power measurement module, providing optimal insulation, while outgoing current is monitored using clamp-on current sensing transformers and through-hole Hall-effect sensors. The signals from the current sensing transformers are converted to digital signals by the ADC, which can then be read via the Raspberry Pi’s Serial Peripheral Interface (SPI) pins. The data is stored in Direct Memory Access (DMA) for fast data capture. The power meter sensor communicates with the Raspberry Pi through an RS485 Modbus connector. The block diagram for the device is shown below (Figure 13).

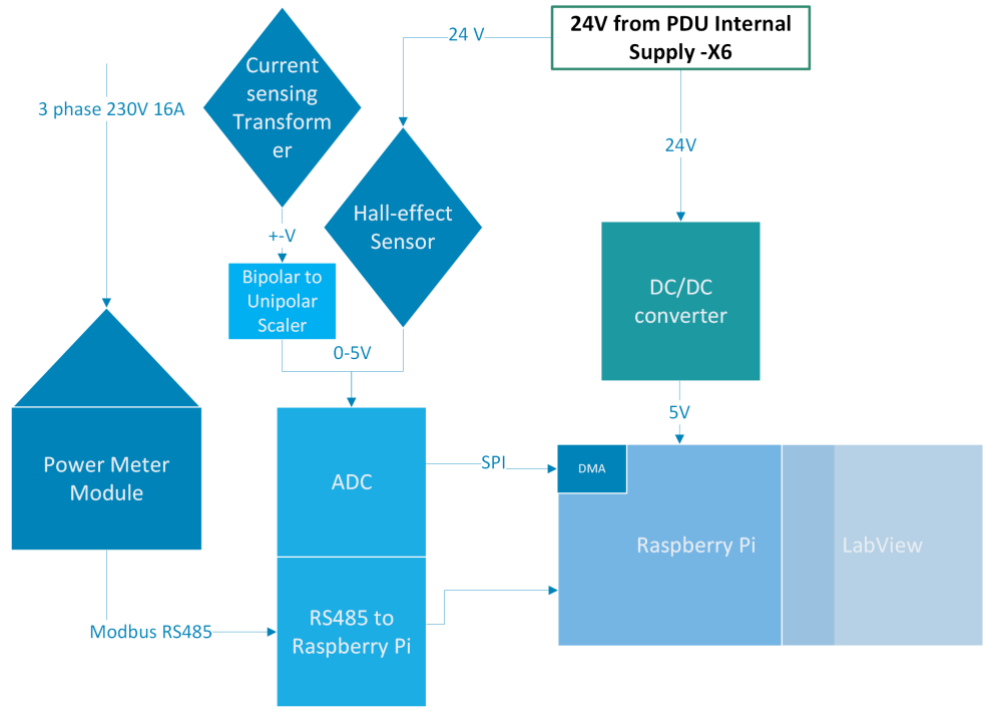

Figure 13. Hardware Block Diagram.

6.2.6 Isolating Casing for the Raspberry Pi

The Raspberry Pi was placed in a DIN mountable casing to prevent potential issues and improve the setup's reliability. This precaution helps minimise the risk of unwanted complications, such as accidental short circuits or physical damage caused by contact with external objects. The open-top design allows modules to be inserted on top of the Raspberry Pi (Figure 14).

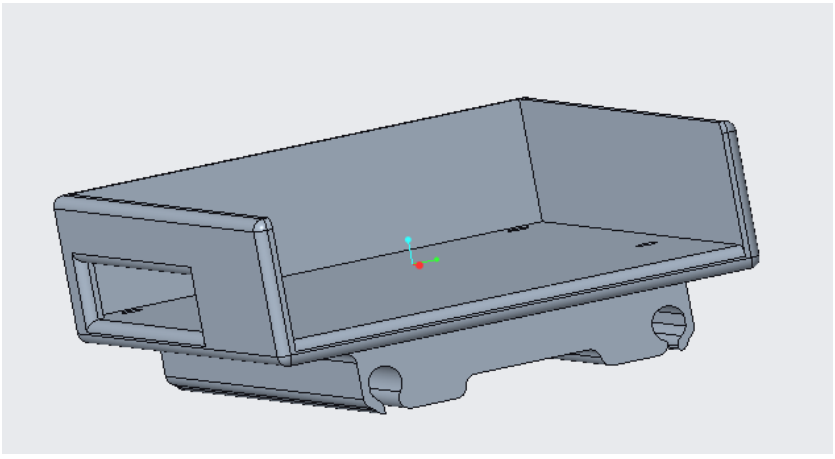

Figure 14. Case For Raspberry Pi.

Figure 15 below shows the prototype. The sensors are not visible as they are outside the picture's frame. The scaling circuit was assembled on a prototype board equipped with feet for attachment to the RS485 module. To streamline the design, reduce size, and minimise complications, this circuit should be implemented on a printed circuit board (PCB). Integrating the ADC and Modbus board with the scaling circuit into a single PCB would further enhance efficiency and functionality.

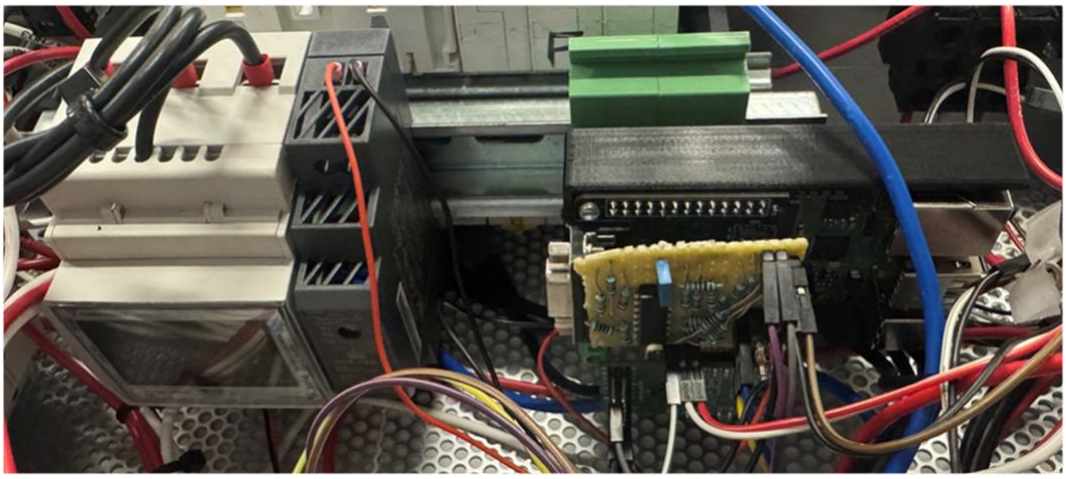

Figure 15. Finished Device Without Sensors.

6.3 Software Development

The initial step was obtaining a compatible image for the Raspberry Pi. Using the Raspberry Pi Foundation's official imager toolkit and a microSD card, an image with LabVIEW 2022 preinstalled was used. This toolkit supports installing first-party and third-party images onto external memory devices. Once the image was written to the microSD card and plugged into the Raspberry Pi, the installation was completed automatically.

Device verification included testing the SPI interface on the RS485 module/GPIO shield. This was achieved by connecting the module's MOSI pin to its MISO pin and running a script to send and read data. Matching outgoing and incoming data confirmed the correct functioning and assignment of the SPI ports. The Modbus interface was verified by sending simple ASCII data messages from a PC using

a simple USB to RS485 connector and verifying the messages on a command prompt connected to the Raspberry Pi.

Only after verifying the hardware could the software development proceed with confidence.

6.3.1 Communicating with the Raspberry Pi

After installation, it was possible to connect to the Raspberry Pi externally. The simplest option was using an ethernet cable on the Raspberry Pi, which was then connected to the same router that the controlling PC used. The Raspberry Pi required to have its Secure SHell (SSH) enabled for this. SSH is a remote access software that allows encrypted connections between systems [26]. In cases where the Raspberry Pi should be connected straight to a PC, a Dynamic Host Configuration Protocol (DHCP) would be necessary.

6.3.2 Programming Language

The programming language was chosen based on compatibility with existing systems and ongoing development. LabVIEW, the department's primary development software, was selected for its familiarity and integration.

Two external LabVIEW libraries were used to accelerate development: the Hobbyist Toolkit (previously known as LINX) for communication with the Raspberry Pi and the NI Modbus Library for interfacing with the Modbus-powered power meter.

The initial plan was to use the Hobbyist Toolkit’s built-in SPI interface, which proved inadequate as it could not achieve the necessary speeds for capturing accurate voltage waveforms. As a result, the Hobbyist Toolkit was limited to hosting the LabVIEW environment on the Raspberry Pi, and an alternative method was used to meet the requirements.

Below is the central LabVIEW block diagram (Figure 16), which has been streamlined by organising functionality into multiple sub-VIs wherever appropriate. Sub-VIs are like standard VIs, the only difference being the calling hierarchy [27]. They help simplify the main code, enhance readability, and facilitate debugging.

LabVIEW also allows for the creation of simultaneous loops. The software automatically allocates processor cores to these loops, enabling them to run simultaneously. This feature makes LabVIEW particularly powerful for handling parallel tasks in complex systems. [28.]

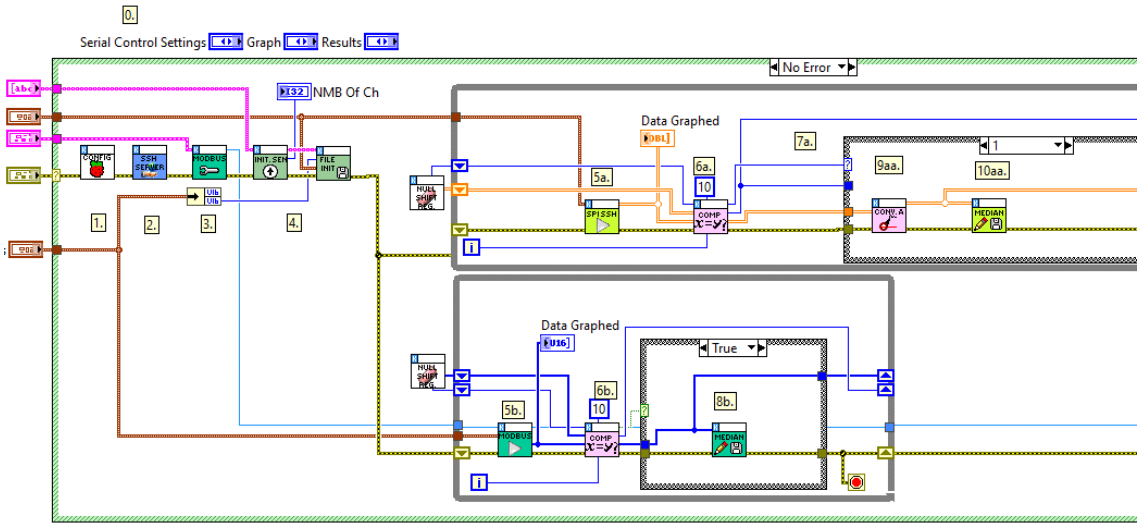

Figure 16. Part of Main VIs Block Diagram.

One of the many sub–VIs was dedicated to converting measured voltage to current based on sensor type (Figure 17). A low-pass filter was added to reduce the noise caused by sampling in the measurements.

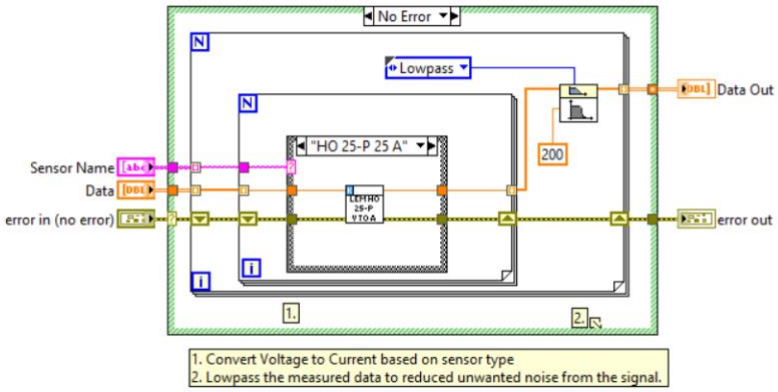

Figure 17. Sub VI was handling Measured Voltage Conversion.

The user interface consists of three panels, with subpanels accessible by the tab at the top (Figure 18). The leftmost panel applies settings for the different serial protocols and Raspberry Pi, while the one in the middle shows numeric results. The panel on the right shows the active graph for these measurements. This user interface was only used in development, as the finished product ran by itself and only logged data to internal files.

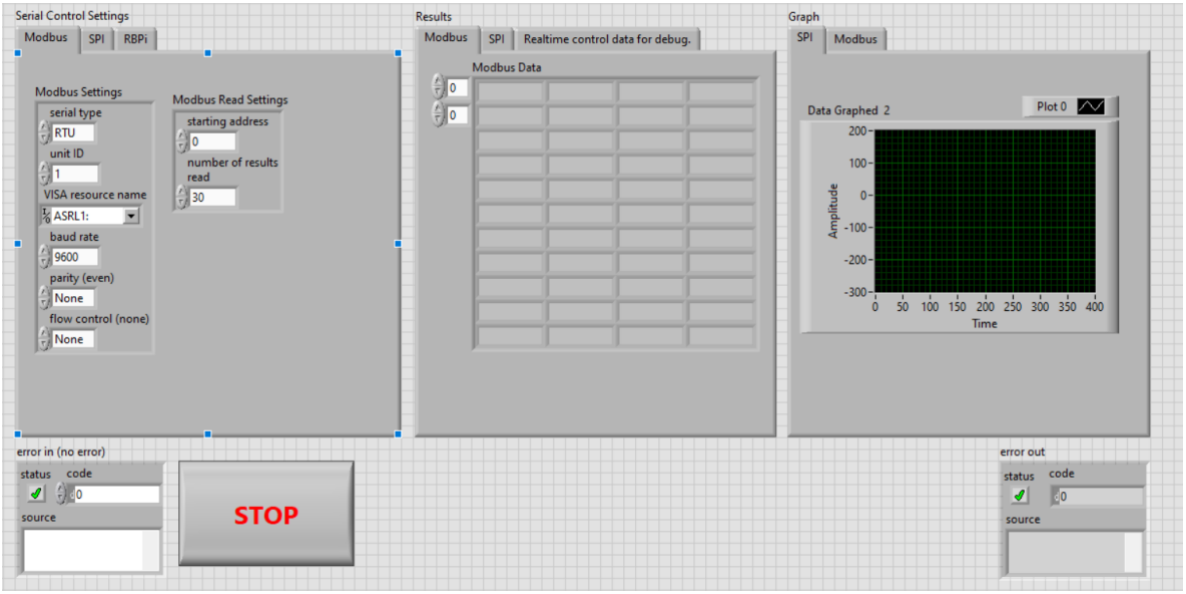

Figure 18. Main VIs User Interface Used for Device Development.

6.3.3 Program Flow

Below is the software's high-level flow diagram (Figure 19). White represents file access, dark blue indicates communication with Modbus, turquoise corresponds to SPI control, and light blue represents Raspberry Pi control.

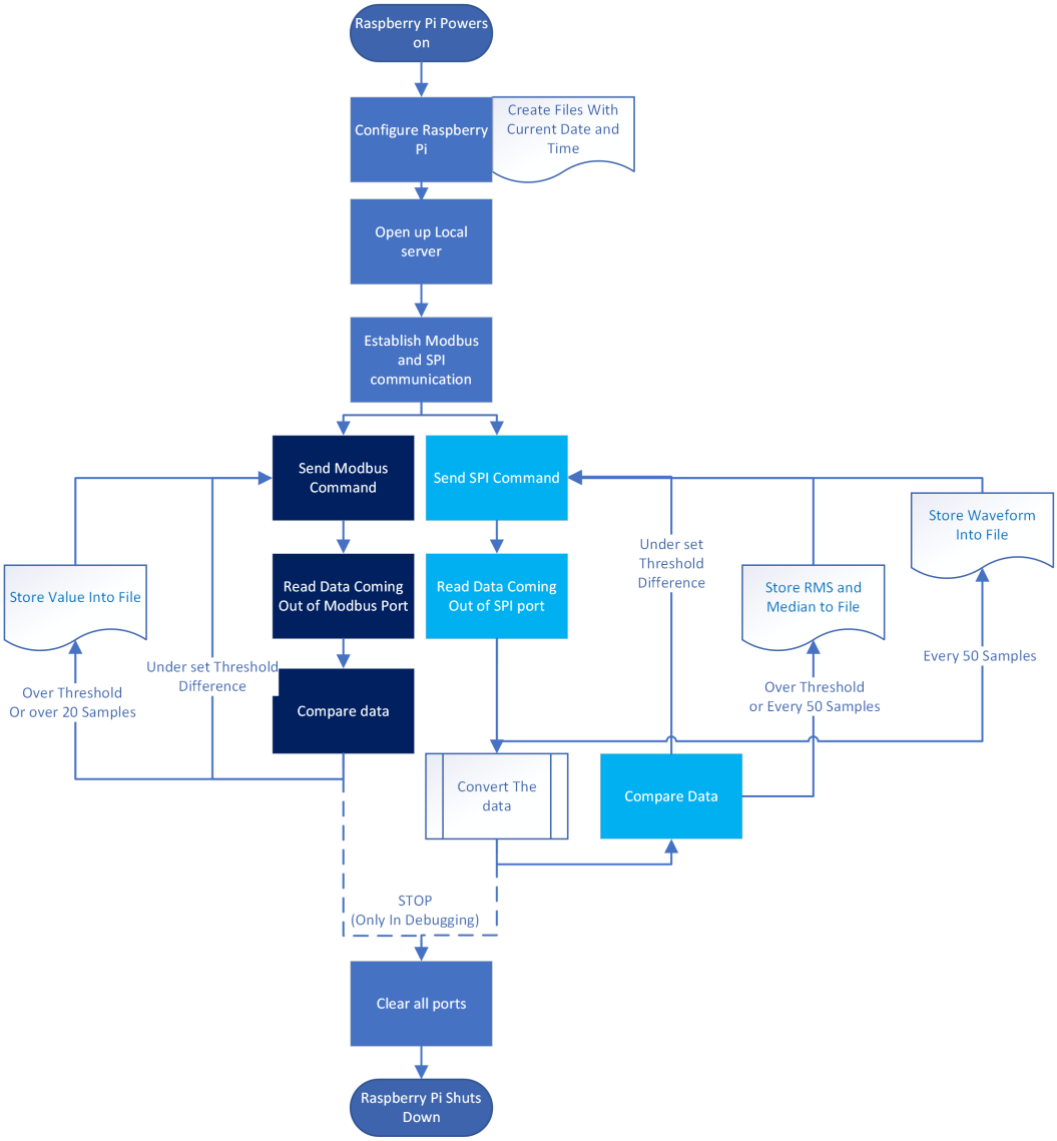

Figure 19. Software Flow Diagram.

The program starts by initialising all devices and configuring port data lines, beginning with the Raspberry Pi. After initialisation, it operates within two continuous loops: one dedicated to communicating with the ADC and the other focused on communicating with the power meter.

Both loops follow a similar structure. They compare the current results to the last saved measurement or check the number of measurements that have elapsed since the previous data point was recorded. Based on these conditions, the program saves the data to files as needed.

The ADC loop includes an additional feature that saves the entire waveform after every 50 samples. This functionality enables later analysis of the captured waveforms.

If the program is stopped from the debugging interface, the while loops exit, and the program continues to a cleanup phase.

6.3.4 Modbus Communication

The RS485 interface in the power meter supports standard MODBUS functions. Implemented functions include reading and writing holding and input registers, diagnostics, and broadcast mode. Key functions like Read Holding Registers (03h) and Read Input Registers (04h) allow data retrieval, while Write Single Holding Register (06h) enables configuration settings. Diagnostics (08h) checks communication integrity, and broadcast mode permits commands to all connected devices without individual responses. [29, 3-6.]

The MODBUS protocol includes several functions for our power meter, including [29, 3-5]:

- Reading Holding Registers (Function Code 03h) - This function reads data from a sequence of holding registers. A typical use might involve reading up to 50 registers in a single request, with data packed in MSB and LSB format.
- Reading Input Registers (Function Code 04h) - Similar to Function 03h, this function reads data from input registers, allowing access to real-time monitoring data.
- Writing Single Holding Register (Function Code 06h) - This function writes data to a single register, which helps set configuration parameters or control outputs.

- Diagnostic (Function Code 08h, Sub-Function 00h) - This diagnostic function allows loopback testing to verify communication integrity.
- Broadcast Mode (Address 00h) - This mode enables the controller device to communicate with all connected devices without expecting individual responses. It is used for one-way commands, reducing the network's response load.

The power meter sends data to the host by writing data into different registers. Appendix 1 lists these addresses and the data they carry.

6.3.5 SPI Protocol

Efficient communication with the AD7490 ADC was essential. To send the correct messages, it was necessary to configure the control register, a 12-bit write-only register that oversees the device’s operational parameters for each conversion. The control register configuration is transferred serially through the Data In (DIN) line while the conversion result is simultaneously read through the Data Out (DOUT) line. [24, 12-13.] Note that this DOUT is always one cycle behind the DIN line.

Data transfer to the control register is synchronised with the falling edge of the Serial Clock (SCLK) signal, and a complete transfer requires 16 SCLK pulses. Only the first 12 bits are written to the control register following the Chip Select (CS) line falling edge, while the remaining four are ignored. The Most Significant Bit (MSB) is transferred first, with specific bits performing various configuration functions. [24, 12-13.]

The 12 bits in the AD7490 control register have defined roles [16, 12]:

- Bit 11 (WRITE): Determines whether the following bits are written to the control register. Setting this bit to 1 enables data writing while setting it to 0 leaves the register unchanged.
- Bit 10 (SEQ): Works with the SHADOW bit (bit 3) to control the sequencer's functionality. This may allow for multiple consecutive conversions without reconfiguring the control register.
- Bits 9 to 6 (ADD3-ADD0): These four bits specify the analogue input channel to be converted in the next cycle or the final channel in a

sequence, with the selection activated on the 14th falling edge of SCLK.

- Bits 5 and 4 (PM1, PM0): Manage the device's power mode. Each bit combination represents a different mode, allowing for power optimisation in various operational states.
- Bit 3 (SHADOW): Alongside SEQ, this bit controls access to the Shadow register, which enables advanced sequencing modes.
- Bit 2 (WEAK/TRI): Determines the state of the DOUT line post-conversion. When set to 1, the DOUT line weakly drives to the ADD3 channel address, while setting it to 0 forces it into a three-state mode.
- Bit 1 (RANGE): Defines the input voltage range for conversion. When set to 0, the range is 0 V to 2 × REF IN; when set to 1, it is 0 V to REF IN. This range setting is essential for accommodating the expected signal amplitude within the ADC's input range.
- Bit 0 (CODING): Selects the output coding scheme, with 0 indicating two’s complement and 1 representing straight binary. This option aligns the ADC output format with the system’s data interpretation requirements.

To accurately capture AC, it is not enough to call for the voltage at a certain point, but rather, the signal needs to be captured for a time equal to or greater than its cycle. As stated by the Sampling Theorem, also known as the Nyquist Theorem, to preserve the full information in the signal, it must also be sampled at a frequency greater than twice its maximum frequency [30].

Direct Memory Access (DMA) is required to capture data reliably at this rate. DMA allows data transfer between memory and peripherals without CPU intervention, using bus memory addresses that require translation from the virtual addresses used by programs. DMA data must reside in uncached memory to ensure correct operation and avoid fetching stale data, as the CPU initially writes to an on-chip cache. Compiler optimisations may also skip memory reads, requiring the `volatile` qualifier to ensure accurate variable access. DMA operates through Control Blocks (CBs), which define the source, destination, and data size and can chain CBs for sequential tasks. Triggered by peripheral requests or running continuously, improper DMA configuration can lead to system crashes, data corruption, or hardware malfunctions. [31.]

Below is part of the C code used to transmit and receive data. It was written in C to provide efficient low-level access to DMAs. A snippet of the code, including the send and receive functions, can be seen below in Listing 1. These messages are not directly written to the ADC but go through the previously discussed DMA registers.

```
// Return Tx data
int ad7490_tx_data(void *buff, int adc_channel)
{
    int chan = adc_channel;
    // First bytes: 10cccc11, (c for channel) // Second bytes: 0001xxxx,  //
Final completion of transfer
    uint8_t txd[3] = {0x80 | ((chan) << 2)| 0x03, 0x10, 0x00};
    memcpy(buff, txd, sizeof(txd));
    return(sizeof(txd));
}

// Return value from ADC Rx data
int ad7490_rx_value(void *buff)
{
    uint8_t *rxd=buff;
    return((int) (((rxd [3] << 8) | (rxd[4]) ) & 0x0fff)); //Return
measurement data with channel number removed.
}
```

Listing 1. Functions for sending and receiving data through SPI.

6.3.6 Linux Command Inside the Hobbyist Toolkit Environment

The Hobbyist Toolkit operates within a virtual machine in the */chroot/nationalinst/labview* directory [32]. Due to this, direct file access using LabVIEW's built-in tools is not possible.

This problem can be overcome using the "chroot SSH Trick", which allows LabVIEW to execute commands outside its chroot environment on Hobbyist Toolkit targets, such as Raspberry Pi, enabling interaction with external tools. This is achieved by installing an SSH client within the chroot, setting up public key authentication for access, and configuring the SSH client to recognise the local host [33.]

Once configured, commands can be executed on the host system from within the LabVIEW chroot using the following commands with LabVIEW System Exec VI:

- *“ssh pi@localhost”* For establishing communication.
- ”*touch filename.txt*” For creating a file.
- ”*cat >> filename.txt*” For writing to the end of an existing file.
- “*more filename.txt*” For printing the content of a file to the terminal.

This trick was also used to communicate with the previously discussed script (SPI Protocol).
Commands for communicating with the program included:

- “sudo *./SPIRead*” For running the script.
- “-R” For setting sample rate.
- “-N” For setting the number of samples to be captured.
- “-C” For setting the channel to be read.

These commands were added to LabVIEW to make communication easier.

6.3.7 The Scale of Finished Software

The final software comprised of the C program and around 50 individual VIs and sub-VIs, many of which were reused multiple times. Most VIs include front panels and accompanying documentation.

During development, real-time measurements could be read or transferred via a local server hosted on the Raspberry Pi. When connected to an external LabVIEW client, they could be monitored in real-time through its user interface.

6.4 Calibration and Baseline Measurements

The initial idea was to use a laptop charger or another consumer electronics device as a load for the initial calibration. However, this approach was quickly deemed impractical, as the current load from a single laptop charger was negligible. The only way to generate a sufficiently large current using this method was to connect multiple devices via an extension cable, where trying to calibrate the load using multiple power ratings would become problematic. It is also important to note that when attempting to measure current with a clamp meter on

a standard power cable, the incoming and outgoing phases cancel each other out, rendering the measurement ineffective.

Calibration started by using an oscilloscope and verifying that the ADC and the scaling circuit were correctly scaled from 0 to 5 V. Once this was done, the process could proceed to individual current sensors, starting with the KEMET CT 3010 current transformer.

The signals below in Figure 20 show the load for a soldering vacuum, soldering iron, and desoldering vacuum.

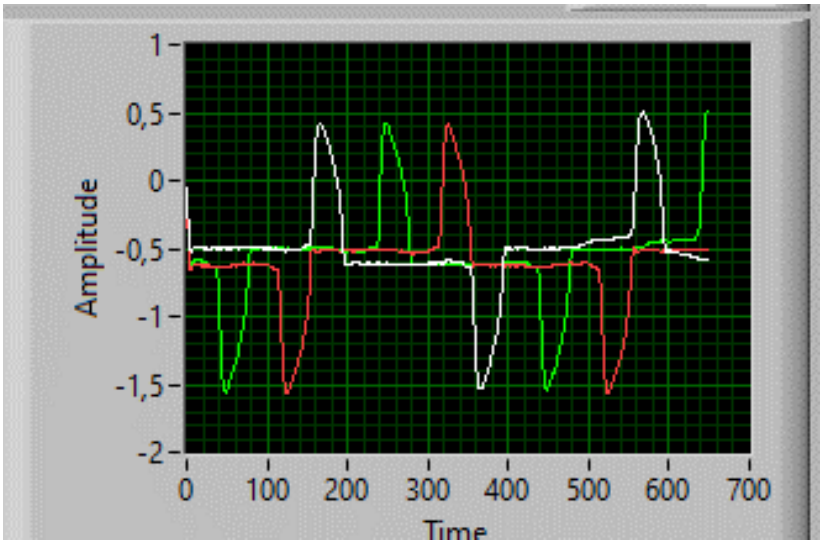

Figure 20. Measured Load Current Transformer.

The phase difference between these signals is caused by the sampling method, which monitors only one channel at a time instead of all three simultaneously. This issue could be resolved by either implementing a timer to continuously run the DMA code and aligning the start of each sample accordingly or modifying the approach to sample all three channels sequentially within each cycle.

The measurement from the current transformer was also verified using a current clamp connected to an oscilloscope (Figure 21). The oscilloscope internally converted the measured voltage to current. After negating the offset and applying

the voltage-to-current conversion based on the datasheet, both methods showed a peak-to-peak value of almost 6 A.

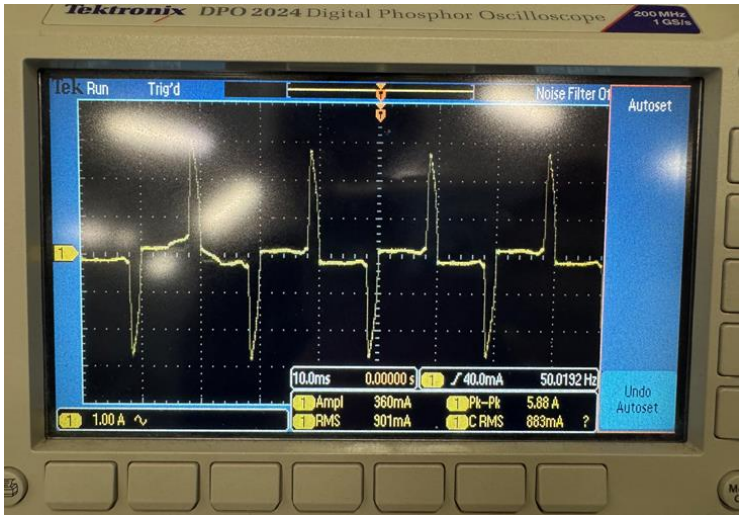

Figure 21. Measured Load Oscilloscope.

The device's power meter indicated a current consumption of 770 mA, while the measured and RMS-converted values were slightly lower, at approximately 730 mA. This discrepancy could be due to minor scaling inaccuracies or the sampling cycle not fully capturing the signal's complete cycle. A 6 mV jump was also detected when the signal crossed the zero point. This behaviour corresponds to the current transformer's datasheet [34, 4] (Figure 22), which specifies a blind spot of around ±3 mV when a 1 kΩ load resistor is used.

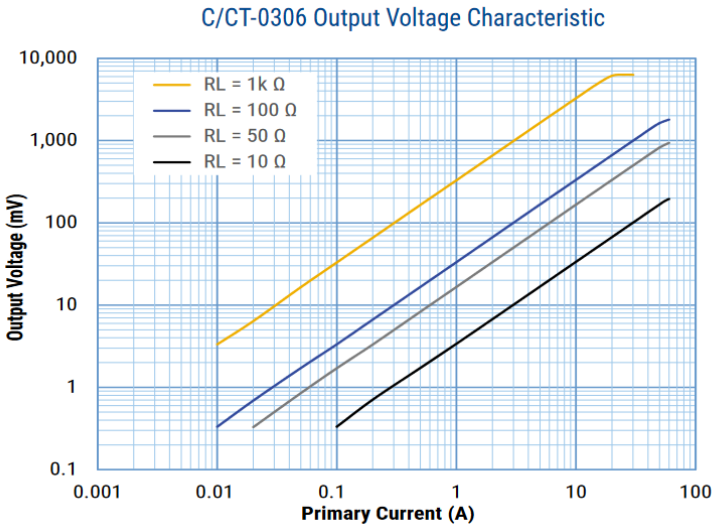

Figure 22. Current transformer Voltage Output Characteristics [34, 4].

6.5 Current Sensor Verification

The measurements from the current sensors and the power meter, conducted during the test station's boot-up, are shown below (Figure 23, Figure 24).

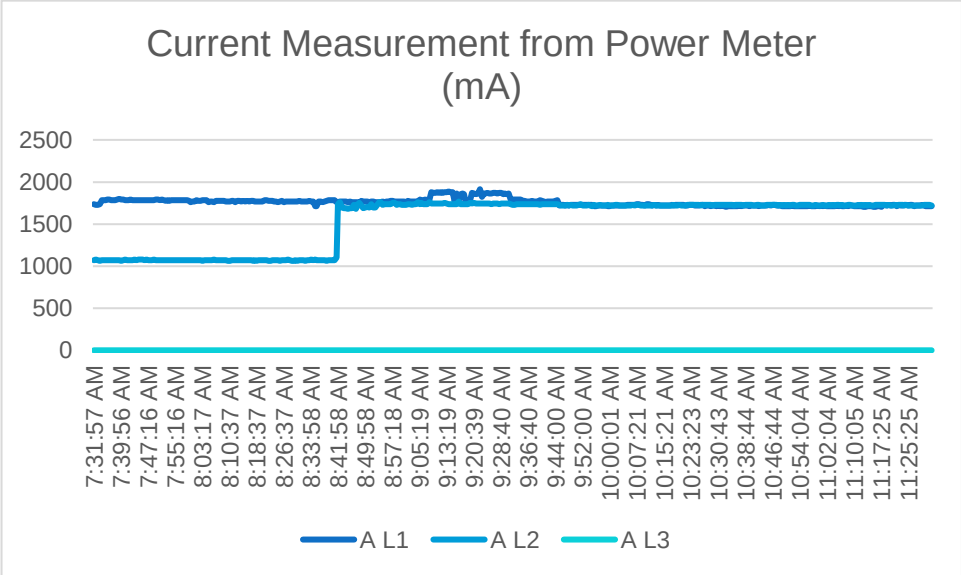

Figure 23. Current Measurement from Power Meter

While the current sensor measurements are less stable, they are still very close to those from the power meter. The slight instability in the current sensor readings is likely due to less filtering and or rounding compared to the more processed values provided by the power meter.

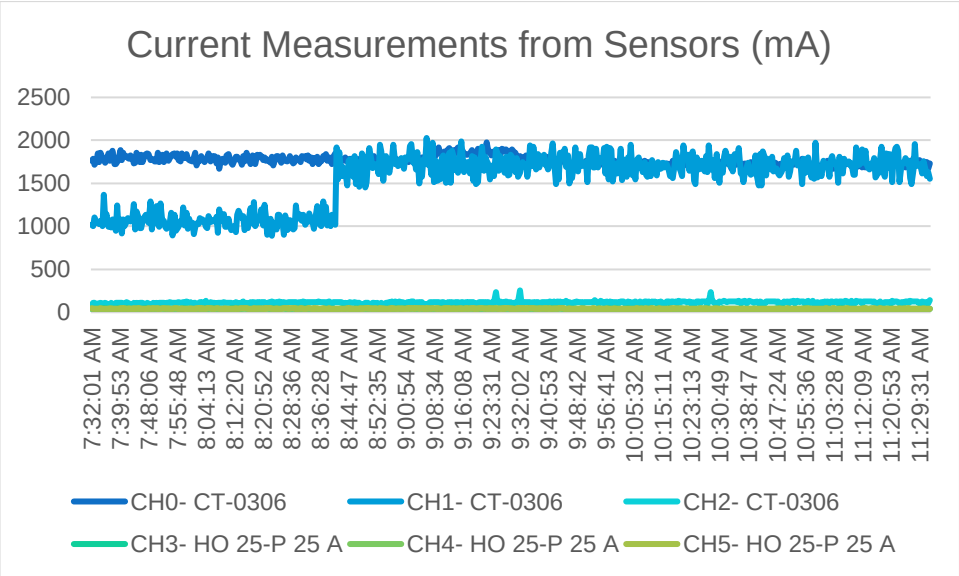

Figure 24. Current Sensor Measurements

The DC measurements from the three Hall-effect sensors (CH3, CH4, and CH5) remained inconclusive since the current load through them remained low.

7 Measurements and Analysis

Measurements included waveforms, energy consumption, power factor and apparent power. Most of the data was collected after the station ran for a while, simulating real-world usage. At this point, the UPS had stabilised itself and consumed power consistently.

The test station used for measurements was not heavily utilised, yet its passive consumption remained relatively high. Two minor consumption peaks were recorded, corresponding to periods of active use of the test station. Outside these peaks, the station remained idle. Notably, all testing equipment in the rack operated continuously, so running tests resulted in only a slight increase in overall consumption.

7.1 Power Measurements from Initial Bootup

Before the UPS was powered on, the consumption on wire L2 was relatively low at 736 W, but after the UPS was turned on, it jumped to 2600 W, where it then stabilised (Figure 25).

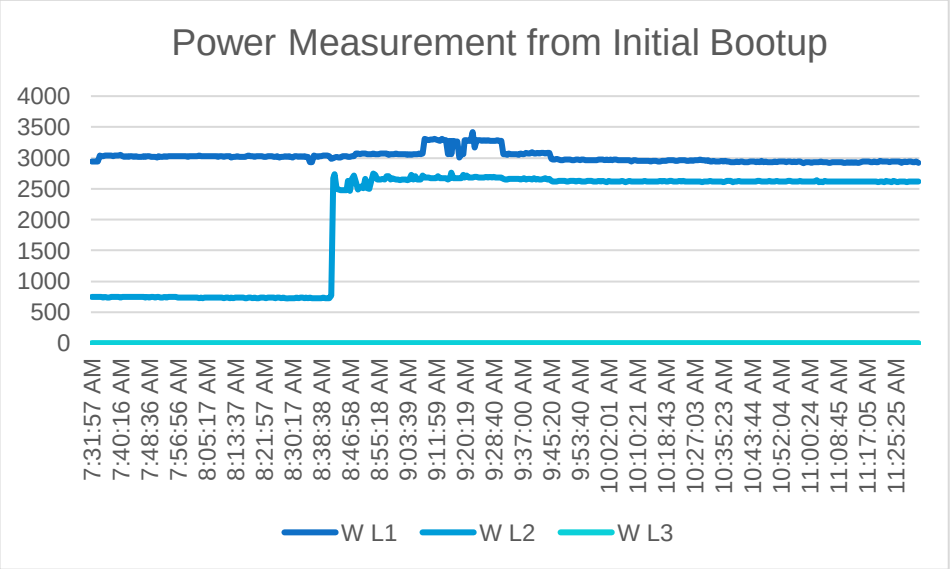

Figure 25. Power Measurement from Initial Bootup.

7.2 Waveform Analysis

Samples were aligned using peak detection, which identified the array index for the delete array function acting as a split operation. After splitting, the signal segments were reassembled into a continuous waveform. At the end of the process, a filter was applied to minimise the noise introduced by the process.

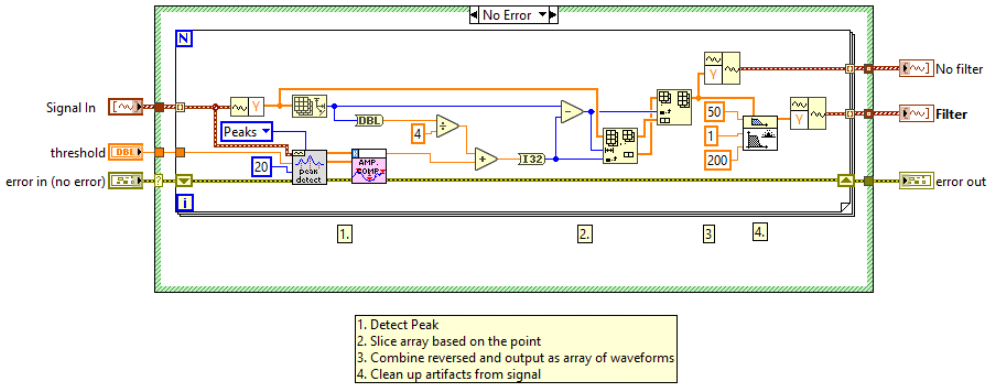

Figure 26. VI for Aligning Signals

Below (Figure 27, Figure 28), the aligned waveforms for L1 (channel 0) and L2 (channel 1) are displayed. Both wires have multiple power sources connected, with L2 also powering the UPS. From these waveforms, we can conclude that the load on both wires remained relatively constant, as the measurements align well, aside from minor noise introduced by the alignment method. This noise can be effectively filtered out.

The amplitude on the y-axis is measured in milliamperes (mA), while the x-axis represents the number of samples.

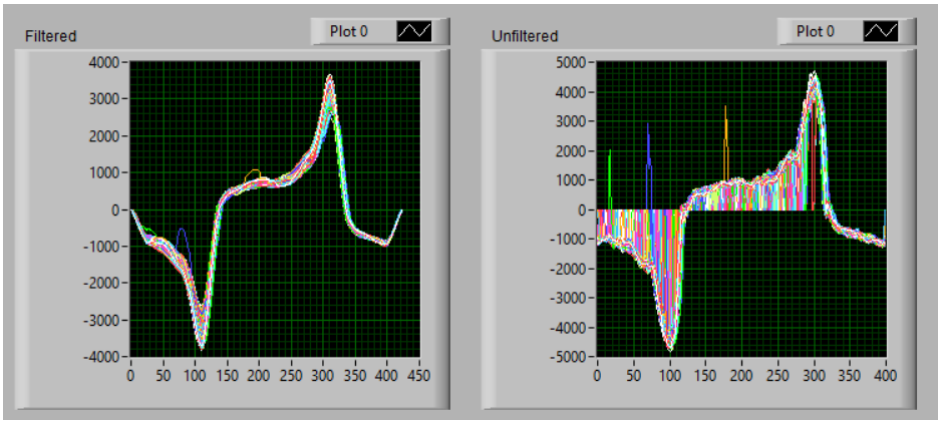

Figure 27. 1000 Aligned Waveforms from L1

Notably, channel one demonstrates a more consistent power consumption pattern, closely resembling a sine wave and thus indicating a more stable operation.

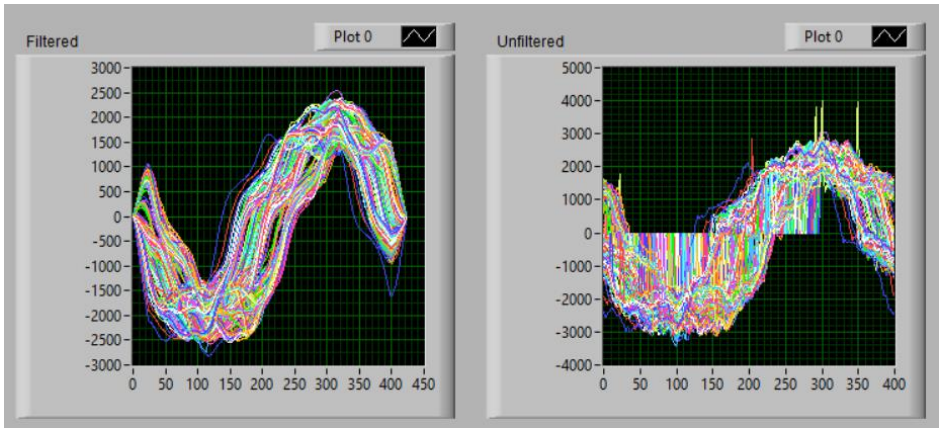

Figure 28. 1000 Aligned Waveforms from L2

Channel two remained unused during these tests, as no power ran through the connector. Thus, the results from this channel solely consist of noise.

7.3 Energy Consumption Analysis

Power consumption remained stable throughout the measurement period (Figure 29). Two peaks were observed during active use on the tester. However, these peaks were relatively insignificant compared to the device's baseline passive consumption.

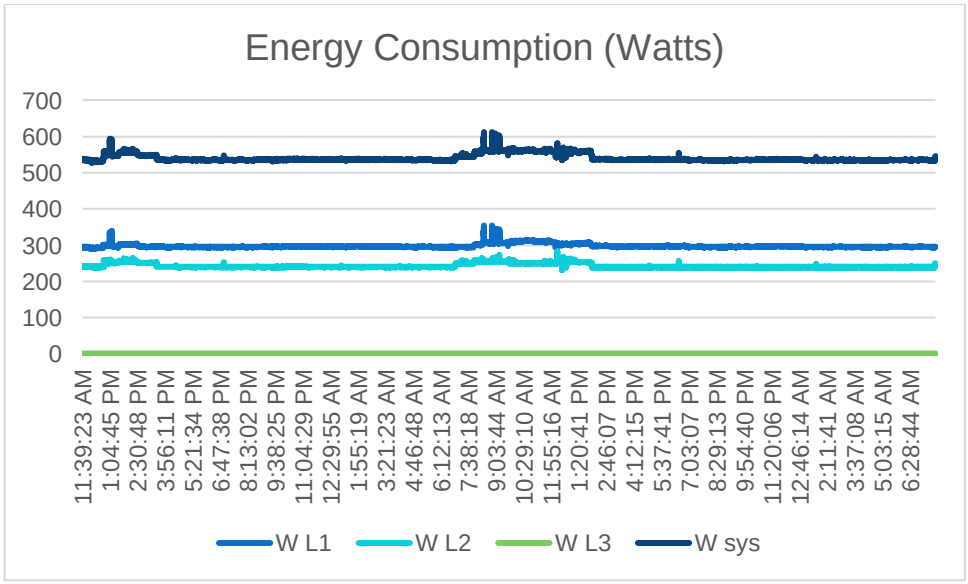

Figure 29. Power Consumption Over Time

Apparent power (Figure 30) remained close to real power.

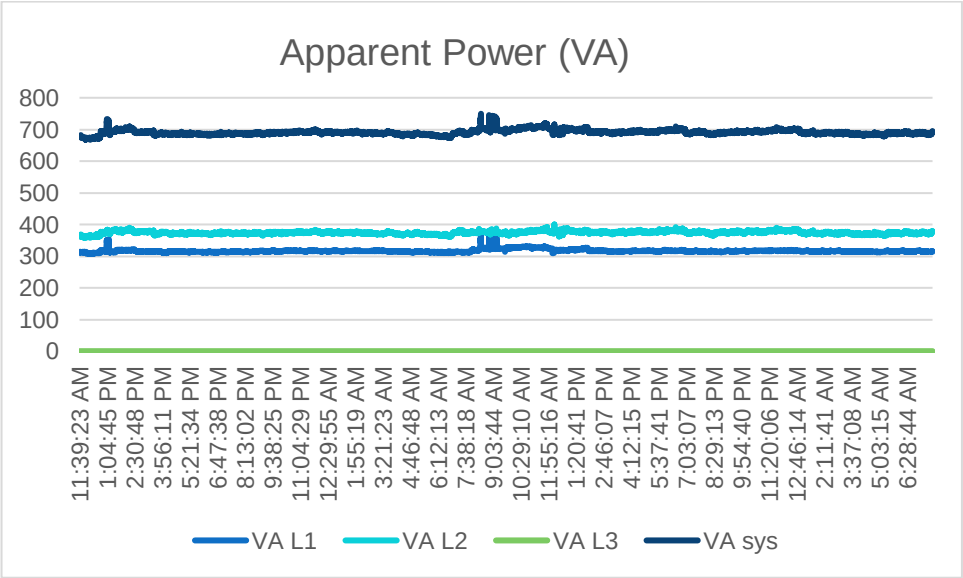

Figure 30. VA Over Time

The power factor is calculated based on the relationship between real and apparent power (see Figure 30).

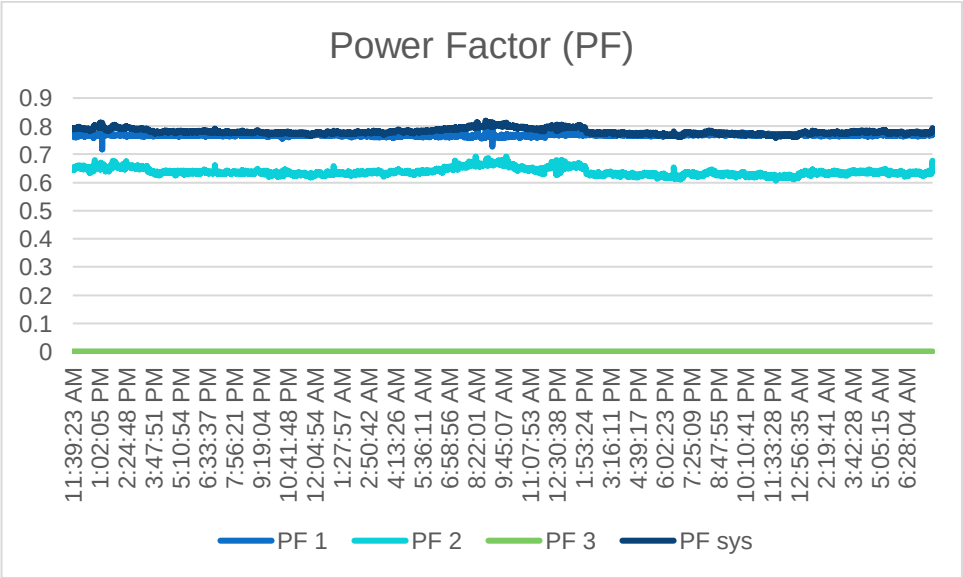

Figure 31. Power Factor Over Time

Values above 0.95 are classified as good, between 0.95 and 0.85 as poor, and below 0.85 as bad [35].

Power factor values from L1 were better than L2. This suggests that while the current consumption from L2 closely resembled a sine wave, it was still out of phase with the voltage, leading to a reduced power factor.

Hourly energy consumption remained stable (Figure 32), with the peaks detected in earlier graphs no longer visible. The plots include individual measurements for each wire and a combined total.

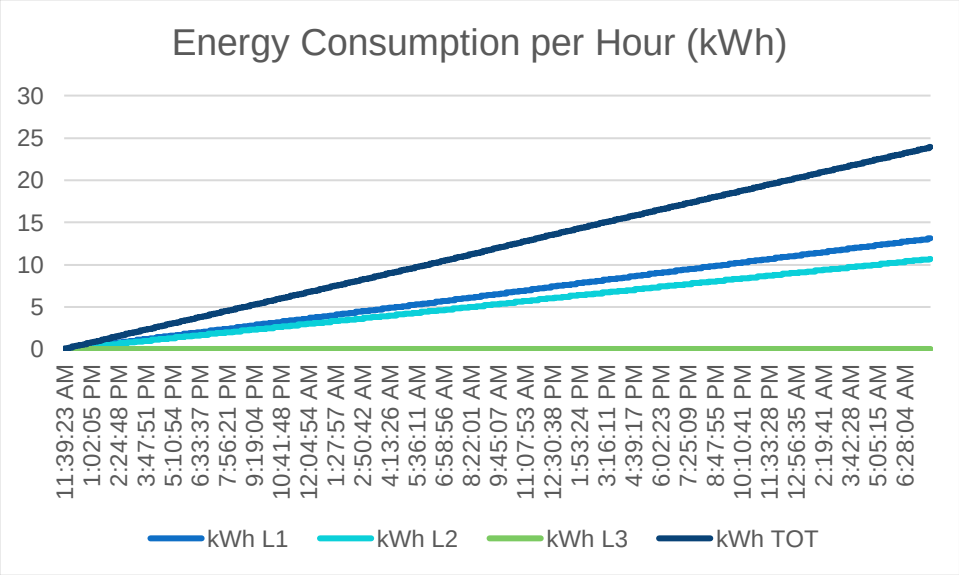

Figure 32. Energy Consumption Over Time

7.4 Calling Fingrid API for Emission Data

With open access to Fingrid's API, various datasets can be retrieved. For this analysis, the focus was on the gCO_2/kWh metric, which calculates the emissions generated by consumption based on the emissions from electricity production during that period. Below is the VI used for calling the API (Figure 33).

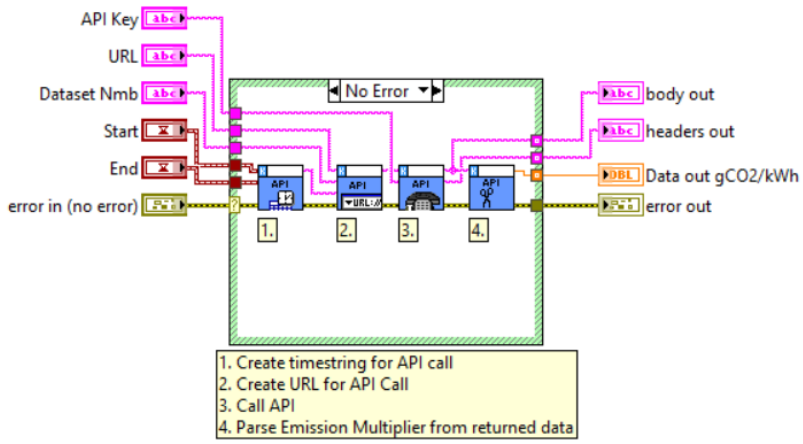

Figure 33. VI for calling Fingrids API.

7.5 Total Emissions and Costs

The total emissions and costs were measured using estimations from the measurements taken. Price (0.00626 €/kWh) and emission multiplier (31.905 gCO_2/kWh) were taken based on the values during the measurement. The results from calculations based on these values are listed below (Table 1).

These prices and emissions can vary significantly depending on the location and timing of the testing equipment, so these results should be considered rough estimates. They also do not consider the costs associated with the extra cooling that may be needed when running these systems continuously in a hot climate.

Table 1. Cost and Emission Estimate for Test System

Time	*Consumption (kWh)*	*Price Estimate (€)* (6)	*Emission Estimate (gCO_2)* (7)
24 Hours	13.1	0.82	316.4
365 Days	4781.5	299.3	115497.1
10 Years	47 815	2994.9	1155604.2

$$Price\ Estimate = Energy\ Consumption * Price\ Per\ kWh \quad (6)$$

$$Emission\ Estimate = \frac{\text{Energy Consumption}}{\text{Emission Multiplier for Domestic Consumption}} \quad (7)$$

To put the emissions into perspective, they were compared to those of passenger cars. The target emissions for passenger cars during 2025–2030 are set at 94 gCO_2/km [36]. According to the equation (8) below, the emissions generated by running the test system for just under 24 hours would be equivalent to driving approximately 3.4 km.

$$Estimation\ \ for\ km\ in\ passenger\ cars = \frac{Total\ Emissions}{Target\ Emissions\ for\ Passenger\ Cars} \quad (8)$$

The projected savings for the test systems, should they be turned off when not in use, are shown below in Table 2. The active state has been defined as 8 hours/day × 5 days/week.

Table 2. Savings If test systems were turned off when idle.

Time	Consumption (kWh)	Price Estimate (€) *(6)*	Emission Estimate (gCO_2) *(7)*
24 Hours	8.7	0.055	278.6
1 Day	69.9	0.44	2229.1
1 Week	3645.5	22.8	116308.6
365 Days	36454.7	228.2	1163085.6

This table highlights the substantial energy consumption of the test station during idle periods over its lifespan. The data from booting up the device (Figure 25) also indicates that turning off the test station when it is not in operation is an energy-efficient option, as the extra power consumption from startup is minimal.

8 Conclusion and Future Development

In this project, a prototype capable of monitoring and logging energy consumption was successfully developed, offering valuable insights into power usage patterns. The design integrated power measurement systems, such as current sensors and a power meter, ensuring accurate data collection. Measurements included energy consumption, power factor and apparent power, demonstrating that even idle systems exhibit relatively high passive consumption. Peaks in consumption were linked to active use, although the overall impact on energy consumption remained minor due to the continuous operation of the testing equipment.

Outgoing DC channel measurements remained inconclusive, as their current draw remained low. This indicates their insignificance in the greater picture of the test stations' consumption; thus, they could be omitted from further development. For waveform capturing, transitioning from a prototype scaling circuit to a more stable PCB design will enhance reliability and reduce complications.

The findings underscore the environmental impact of idle test systems, which, when scaled across multiple stations, can contribute significantly to emissions and costs. Addressing this issue through improved energy management will help achieve sustainability goals.

The captured waveforms have opened the topic of improving power factor correction by reducing the total harmonic distortion, which could further improve efficiency and system reliability. With one phase often unused in the PDU, there is potential for improvement by redistributing the load evenly across all three phases.

This project lays the groundwork for advancing PDU design, emphasising the importance of energy efficiency and sustainability. As the industry moves towards more environmentally conscious practices, these improvements will contribute to meeting future energy and emissions targets.

References

1 National Instruments, Fundamentals of Building a Test System, 2020.

2 Worton. *fs.com.* 29 May 2020. Accessed 3 October 2024. https://community.fs.com/article/guide-to-power-distribution-unit.html

3 National Instruments. *ni.com.* Accessed 24 November 2024. https://www.ni.com/pdf/product-flyers/rack-mountable-power-distribution-units.pdf

4 Ormazabal. *ormazabal.com.* Accessed 17 September 2024. https://www.ormazabal.com/en-gb/what-is-a-ups-and-how-does-it-work-2-2/

5 KONE Oyj. *kone.fi*. Accessed 15 September 2024. https://www.kone.fi/tietoa-meista/kone-yrityksena/

6 KONE Oyj. *kone.fi*. Accessed 15 September 2024. https://www.kone.fi/tietoa-meista/kone-yrityksena/ymparisto/

7 KONE Oyj. *kone.com.* Accessed 15 September 2024. https://www.kone.com/en/news-and-insights/stories/testing-elevators-underground-and-remotely.aspx

8 U.S. Energy Information Administration. *eia.gov.* 29 November 2022. Accessed 5 October 2024. https://www.eia.gov/energyexplained/electricity/measuring-electricity.php

9 Electrical Technology. *electricaltechnology.org.* Accessed 6 October 2024. https://www.electricaltechnology.org/2013/07/active-reactive-apparent-and-complex.html

10 All About Circuits. *allaboutcircuits.com.* Accessed 5 October 2024. https://www.allaboutcircuits.com/textbook/alternating-current/chpt-11/true-reactive-and-apparent-power/

11 Electrical Technology. *electricaltechnology.org.* Accessed 9 October 2024. https://www.electricaltechnology.org/2016/05/importance-of-reactive-power.html

12 Fluke. *fluke.com.* Accessed 7 October 2024. https://www.fluke.com/en-us/learn/blog/power-quality/single-phase-vs-three-phase-power?srsltid=AfmBOory-qZog9ixn5OjKkxkp6bMOSCTrBb4PPpEE_Fni_GGfDHtWUgj

13 Howard. *fs.com.* 17 December 2020. Accessed 5 October 2024. https://community.fs.com/article/single-phase-vs-three-phase-ups-whats-the-difference-and-how-to-choose.html

14 ATO. *voltagestabilizer.org.* Accessed 11 October 2024. https://www.voltagestabilizer.org/3-phase-3-wire-vs-3-phase-4-wire-voltage-stabilizer

15 Jason Sachs. *embeddedrelated.com.* 23 December 2018. Accessed 21 November 2024. https://www.embeddedrelated.com/showarticle/1213.php

16 ON Semiconductor, Power Factor Correction (PFC) Handbook, Denver: SCILLC, 2014.

17 Fingrid. *fingrid.fi*. Accessed 7 October 2024. https://www.fingrid.fi/sahkomarkkinainformaatio/co2/

18 Monolithic Power *monolithicpower.com*. Accessed 5 December 2024. https://www.monolithicpower.com/en/learning/resources/current-sensors-types-key-parameters-performance-comparison-and-common-applications

19 S. K. Sahdev, Basic Electrical Engineering, Delhi: Pearson Education, 2015.

20 Electronics Notes. *electronics-notes.com.* Accessed 20 November 2024. https://www.electronics-notes.com/articles/test-methods/measurement-techniques/current-sense-transformer.php

21 RS Components. *se.rs-online.com*. Accessed 10 October 2024. https://se.rs-online.com/web/generalDisplay.html?id=ideas-and-advice/hall-effect-sensors-guide

22 Electronics Tutorials. *electronics-tutorials.ws.* Accessed 1 November 2024. https://www.electronics-tutorials.ws/electromagnetism/hall-effect.html

23 Raspberry Pi. *raspberrypi.com.* Accessed 1 October 2024. https://www.raspberrypi.com/about/

24 Analog Devices, Data Sheet AD7490, 2021.

25 Equustek. *equustek.com.* 2 March 2018. Accessed 10 October 2024. https://www.equustek.com/modbus-rs485-everything-need-know/

26 Linux. *www.linux.fi.* Accessed 2024 November 18. https://www.linux.fi/wiki/SSH

27 Labviewwiki. *labviewwiki.org.* 7 August 2024. Accessed 2 December 2024. https://labviewwiki.org/wiki/SubVI

28 National Instruments. *ni.com.* Accessed 20 November 2024. https://www.ni.com/en/shop/labview/multicore-programming-with-ni-labview.html?srsltid=AfmBOop5RmsWdeJAnzoeWrEPCrOdBLusWeBrTaf6JslddB53hZMWAWt

29 Carlo Gavazzi, Communication Protocol, 2021.

30 T. Z. &. P. Shah. *egr.uh.edu.* Accessed 12 November 2024. http://www2.egr.uh.edu/~glover/applets/Sampling/Sampling.html

31 J. P. Bentham. *iosoft.blog.* 2020. Accessed 12 November 2024. https://iosoft.blog/2020/06/11/fast-data-capture-raspberry-pi/

32 Rolfk. *ni.com.* 3 January 2021. Accessed 11 November 2024. https://forums.ni.com/t5/Hobbyist-Toolkit/Save-to-file-on-raspberry-pi-using-Linx/td-p/4131929

33 LabVIEW Makerhub. *labviewmakerhub.com*. Accessed 11 December 2024. https://www.labviewmakerhub.com/doku.php?id=learn:libraries:linx:misc:chroot-ssh-trick#dokuwiki__top

34 Kemet, C/CT, High Current AC, Snap-on Type, Yageo, 2023.

35 S. Mugo. *eepower.com.* 22 September 2022. Accessed 8 December 2024. https://eepower.com/technical-articles/power-factor-determining-how-much-electricity-your-power-system-consumes/

36 J. D. a. P. M. Uwe Tietge. *theicct.org.* 18 September 2024. Accessed 6 December 2024. https://theicct.org/publication/co2-emissions-new-pv-europe-car-manufacturers-performance-2023-sept24/

List of Modbus Data Addresses for the Power Meter [29, 9-10.]

MODBUS: read only mode with functions code 03 and 04 Table 2.4-1

Modicom address	Physical address	Length (words)	VARIABLE ENG. UNIT	Data Format	Notes
300001	0000h	2	V L1-N	INT32	Value weight: Volt*10
300003	0002h	2	V L2-N	INT32	
300005	0004h	2	V L3-N	INT32	
300007	0006h	2	V L1-L2	INT32	
300009	0008h	2	V L2-L3	INT32	
300011	000Ah	2	V L3-L1	INT32	
300013	000Ch	2	A L1	INT32	Value weight: Ampere*1000
300015	000Eh	2	A L2	INT32	
300017	0010h	2	A L3	INT32	
300019	0012h	2	W L1	INT32	Value weight: Watt*10
300021	0014h	2	W L2	INT32	
300023	0016h	2	W L3	INT32	
300025	0018h	2	VA L1	INT32	Value weight: VA*10
300027	001Ah	2	VA L2	INT32	
300029	001Ch	2	VA L3	INT32	
300031	001Eh	2	var L1	INT32	Value weight: var*10
300033	0020h	2	var L2	INT32	
300035	0022h	2	var L3	INT32	
300037	0024h	2	V L-N sys	INT32	Value weight: Volt*10
300039	0026h	2	V L-L sys	INT32	
300041	0028h	2	W sys	INT32	Value weight: Watt*10
300043	002Ah	2	VA sys	INT32	Value weight: VA*10
300045	002Ch	2	var sys	INT32	Value weight: var*10
300047	002Eh	1	PF L1	INT16	Negative values correspond to exported active power, positive values correspond to imported active power. Value weight: PF*1000
300048	002Fh	1	PF L2	INT16	
300049	0030h	1	PF L3	INT16	
300050	0031h	1	PF sys	INT16	
300051	0032h	1	Phase sequence	INT16	The value “1” corresponds to L1-L3-L2 sequence, the value 0 corresponds to L1-L2L3 sequence. The phase sequence value is meaningful only in a 3-phase system
300052	0033h	1	Hz	INT16	Value weight: Hz*10
300053	0034h	2	kWh (+) TOT	INT32	Value weight: kWh*10
300055	0036h	2	Kvarh (+) TOT	INT32	Value weight: kvarh*10
300057	0038h	2	kW dmd	INT32	Value weight: Watt*10
300059	003Ah	2	kW dmd peak	INT32	Value weight: Watt*10
300061	003Ch	2	kWh (+) PARTIAL	INT32	Value weight: kWh*10
300063	003Eh	2	Kvarh (+) PARTIAL	INT32	Value weight: kvarh*10
300065	0040h	2	kWh (+) L1	INT32	Value weight: kWh*10
300067	0042h	2	kWh (+) L2	INT32	Value weight: kWh*10
300069	0044h	2	kWh (+) L3	INT32	Value weight: kWh*10
300071	0046h	2	kWh (+) t1	INT32	Value weight: kWh*10
300073	0048h	2	kWh (+) t2	INT32	Value weight: kWh*10
300075	004Ah	2	kWh (+) t3	INT32	Not available, value =0

300077	004Ch	2	kWh (+) t4	INT32	Not available, value =0
300079	004Eh	2	kWh (-) TOT	INT32	Value weight: kWh*10
300081	0050h	2	kvarh (-) TOT	INT32	Value weight: kvarh*10
300083	0052h	2	kWh (-) PARTIAL	INT32	Not available, value =0
300085	0054h	2	Kvarh (-) PARTIAL	INT32	Not available, value =0
300087	0056h	2	kVAh TOT	INT32	Not available, value =0
300089	0058h	2	kVAh PARTIAL	INT32	Not available, value =0
300091	005Ah	2	Run hour meter	INT32	Value weight: hours*100, only ET series and EM330
300093	005Ch	2	Run hour meter kWh (-)	INT32	Not available, value =0
300095	005Eh	2	n.a.	INT32	Not available, value =0
300097	0060h	2	kWh (-) L1	INT32	Value weight: kWh*10, only ET series
300099	0062h	2	kWh (-) L2	INT32	Value weight: kWh*10, only ET series
300101	0064h	2	kWh (-) L3	INT32	Value weight: kWh*10, only ET series
300103	0066h	2	kWh (+) t5	INT32	Not available, value =0
300105	0068h	2	kWh (+) t6	INT32	Not available, value =0
300107	006Ah	2	kWh (+) t7	INT32	Not available, value =0
300109	006Ch	2	kWh (+) t8	INT32	Not available, value =0
300111	006Eh	2	n.a.	INT32	Not available, value =0
300113	0070h	2	n.a.	INT32	Not available, value =0
300115	0072h	2	n.a.	INT32	Not available, value =0
300117	0074h	2	n.a.	INT32	Not available, value =0
300119	0076h	2	n.a.	INT32	Not available, value =0
300121	0078h	2	n.a.	INT32	Not available, value =0
300123	007Ah	2	n.a.	INT32	Not available, value =0
300125	007Ch	2	n.a.	INT32	Not available, value =0
300127	007Eh	2	n.a.	INT32	Not available, value =0